HHS Public Access

Author manuscript

Ophthalmology. Author manuscript; available in PMC 2017 November 01.

Published in final edited form as:

Ophthalmology. 2016 November ; 123(11): 2309–2317. doi:10.1016/j.ophtha.2016.07.023.

Optical Coherence Tomography Angiography Vessel Density in Glaucomatous Eyes with Focal Lamina Cribrosa Defects

Min Hee Suh, MD[1,2], **Linda M. Zangwill, PhD**[1], **Patricia Isabel C. Manalastas, MD**[1], **Akram Belghith, PhD**[1], **Adeleh Yarmohammadi, MD**[1], **Felipe Medeiros, MD, PhD**[1], **Alberto Diniz-Filho, MD, PhD**[1], **Luke Saunders, PhD**[1], **Siamak Yousefi, PhD**[1], and **Robert N. Weinreb, MD**[1]

[1]Hamilton Glaucoma Center, Shiley Eye Institute, and the Department of Ophthalmology, University of California San Diego, La Jolla, CA, United States

[2]Department of Ophthalmology, Haeundae Paik Hospital, Inje University College of Medicine, Busan, South Korea

Abstract

Purpose—To investigate whether vessel density assessed by optical coherence tomography angiography (OCT-A) is reduced in glaucomatous eyes with focal lamina cribrosa (LC) defects.

Design—Cross-sectional case-control study.

Participants—Eighty-two primary open angle glaucoma (POAG) patients from the Diagnostic Innovations in Glaucoma Study (DIGS) with and without focal LC defects (41 eyes of 41 patients in each group) matched by severity of visual field (VF) damage.

Methods—OCT-A-derived circumpapillary vessel density (cpVD) was calculated as the percentage area occupied by vessels in the measured region extracted from the retinal nerve fiber layer (RNFL) in a 750-μm-wide elliptical annulus around the disc. Focal LC defects were detected using swept-source OCT images.

Main Outcome Measures—Comparison of global and sectoral (eight 45 degree sectors) cpVDs and circumpapillary retinal nerve fiber layer (cpRNFL) thicknesses in eyes with and without LC defects.

*Correspondence should be addressed to Robert N. Weinreb, MD., University of California San Diego, 9500 Gilman Dr, MC 0946, La Jolla, CA 92093, USA; rweinreb@ucsd.edu.

Needs Conflict of interest statement for everyone.

Financial Disclosure(s): Min Hee Suh: none; Linda M. Zangwill: Research support – Carl Zeiss Meditec, Heidelberg Engineering, National Eye Institute, Topcon,; Patricia Isabel Manalastas: none; Akram Belghith: none; Adeleh Yarmohammadi: none; Felipe A. Medeiros: Financial support – Alcon, Allergan, Bausch & Lomb, Carl Zeiss Meditec, Heidelberg Engineering, Merck, Reichert, Sensimed, and Topcon; Research support – Alcon, Allergan, Carl Zeiss Meditec, National Eye Institute; and Reichert; Consultant – Allergan, Carl Zeiss Meditec, and Novartis; Alberto Diniz-Filho: none; Luke Saunders: none; Siamak Yousefi: none; Robert N. Weinreb: Research support –Carl Zeiss Meditec, Genentech, Heidelberg Engineering, National Eye Institute, Optovue, and Topcon; Consultant – Alcon, Allergan, Bausch & Lomb, Carl Zeiss Meditec, Sensimed, and Topcon.

The funding organizations had no role in the design or conduct of this research.

Results—Age, global and sectoral cpRNFL thicknesses, visual field mean deviation and pattern standard deviation, presence of the optic disc hemorrhage, and mean ocular perfusion pressure did not differ between the patients with and without LC defects ($P > 0.05$, for all comparisons). Mean cpVDs of eyes with LC defects were significantly lower than those without a defect globally (52.9 ± 5.6 vs. 56.8 ± 7.7 %, $P = 0.013$), and in the inferotemporal (IT) (49.5 ± 10.3 vs. 56.8 ± 12.2 %, $P = 0.004$), superotemporal (ST) (54.3 ± 8.8 vs. 58.8 ± 9.6 %, $P = 0.030$), and inferonasal (IN) (52.4 ± 9.0 vs. 57.6 ± 9.1 %, $P = 0.009$) sectors. Eyes with LC defects in the IT sector (n = 33) had significantly lower cpVDs than those without a defect in the corresponding IT and IN sectors ($P < 0.05$, respectively). Eyes with LC defects in the ST sector (n = 19) had lower cpVDs in ST, IT, and IN sectors ($P < 0.05$, respectively).

Conclusions—In eyes with similar severity of glaucoma, OCT-A-measured vessel density was significantly lower in POAG eyes with focal LC defects than those without a LC defect. Moreover, reduction of vessel density was spatially correlated with the location of the LC defect.

Although the pathogenesis of glaucoma is not fully understood, the lamina cribrosa (LC) is a putative site of retinal ganglion cell axonal injury.[1–4] Recently, focal LC defects, areas of localized loss of laminar tissue, has been reported to be an important structural feature associated with the glaucomatous visual field (VF) loss.[5–7] Further, there is increasing evidence that focal LC defects may be related to vascular changes of the ONH, including optic disc hemorrhage,[7–9] as well as other ophthalmoscopic structural changes such as neuroretinal rim loss, acquired pits of the optic nerve head (APON), and retinal nerve fiber layer (RNFL) defects.[10, 11] However, little is known about the association between the retinal microvasculature and the presence of focal LC defects, an issue relevant to pathogenesis of glaucomatous optic neuropathy.[12, 13]

Optical coherence tomography angiography (OCT-A) is now available to provide qualitative and quantitative information of the perfused microvasculature of various retinal layers. It has advantages over other techniques such as fluorescein angiography, laser speckle flowgraphy and laser doppler flowmetry by its noninvasiveness and better reproducibility.[14–20] Further, OCT-A-derived quantification of the peripapillary vasculature has been shown to be related to the presence and severity of the glaucoma.[14–16, 21]

The purpose of the present study was to compare the OCT-A-derived peripapillary RNFL vessel density between glaucomatous eyes with and without a focal LC defect.

Materials and Methods

Study Subjects

This was a cross-sectional study involving primary open angle glaucoma (POAG) patients from the Diagnostic Innovations in Glaucoma Study (DIGS) (ClinicalTrials.gov identifier: NCT00221897). The DIGS is an ongoing prospective longitudinal study at the Hamilton Glaucoma Center, University of California, San Diego (UCSD) designed to evaluate optic nerve structure and visual function in glaucoma. Details of the DIGS protocol have been described previously.[22] All methods adhered to the tenets of the Declaration of Helsinki and the Health Insurance Portability and Accountability Act (HIPAA) and were approved by the

Institutional Review Boards at the UCSD. Informed consent was obtained from all participants.

Patients with established POAG who completed OCT-A imaging and ONH imaging using both spectral-domain OCT (SD-OCT) and swept-source OCT (SS-OCT) were included. All participants underwent an ophthalmological examination, including assessment of best corrected visual acuity (BCVA), slit-lamp biomicroscopy, intraocular pressure (IOP) measurement with Goldmann applanation tonometry, gonioscopy, central corneal thickness measured with ultrasound pachymetry (DGH Technology Inc. Exton, PA), dilated fundus examination, simultaneous stereophotography of the optic disc, standard automated perimetry (Humphrey Field Analyer; 24-2 Swedish interactive threshold algorithm; Carl-Zeiss Meditec), SD-OCT, OCT-A, and SS-OCT. Perimetry and all imaging tests were conducted within a 6-month period.

To be included, patients were required to have been diagnosed with POAG, > 18 years of age, BVCA ≥ 20/40, and open angle by gonioscopy. Patients with a history of ocular intervention (except for uncomplicated cataract or glaucoma surgery), intraocular disease (e.g. diabetic retinopathy or non-glaucomatous optic neuropathy), or systemic disease (e.g. stroke or pituitary tumor) that could influence the study results were excluded from the study. Those with systemic hypertension and diabetes mellitus were included unless they were diagnosed with diabetic or hypertensive retinopathy. Eyes with unreliable VF or poor quality imaging tests also were excluded.

POAG was defined as the presence of glaucomatous optic nerve damage (i.e., the presence of focal thinning, notching, localized or diffuse atrophy of retinal nerve fiber layer) and associated repeatable VF damage. Glaucomatous VF damage was defined as a glaucoma hemifield test outside normal limits or a pattern standard deviation outside 95 % normal limits confirmed on two consecutive, reliable (fixation losses and false negatives < 33% and <15% false positives) tests.

Systemic measurements included systolic and diastolic blood pressure (BP) and pulse rate measured at the height of the heart with an Omron Automatic (Model BP791IT) blood pressure instrument. Mean arterial pressure was calculated as 1/3 systolic BP + 2/3 diastolic BP. Mean ocular perfusion pressure (MOPP) was defined as the difference between 2/3 of mean arterial pressure and IOP.

Presence of the disc hemorrhage was determined based on the past follow-up stereophotography at intervals of 12 months. Glaucomatous disc hemorrhage was defined as an isolated splinter or flame-shaped hemorrhage on optic disc tissue or crossing the optic disc.[23] Two independent graders who were masked to patient information and test results independently evaluated each image. Discrepancies between the two graders were resolved by consensus.

Spectral-Domain Optical Coherence Tomography Imaging

All subjects underwent ONH imaging with a commercial SD-OCT system (Avanti; Optovue, Inc., Fremont, CA, USA). Avanti SD-OCT has an A –scan rate of 70-kHz and a light source

with center wavelength of 840 nm. The ONH map protocol calculates circumpapillary RNFL (cpRNFL) thicknesses in a 10 pixel-wide band along a 3.45 mm diameter circle centered on the ONH based on the 360 degree global area and eight 45 degree sectors. Only good-quality images, as defined by scans with a signal strength index ≥ 37, and without segmentation failure or artifacts were included.

Optical Coherence Tomography Angiography Imaging

The OCT AngioVue system (Otovue, Inc., Fremont, CA, USA) incorporated in the Avanti SD-OCT system provides non-invasive visualization of the retinal microvasculature. Details have been described in elsewhere.[14] Briefly, the OCT-A image is directly derived from SD-OCT B-scans. Specifically, the SD-OCT image consists of a series of B-scans with 2 rapid repeats at each B-scan location, and the average of the 2 repeated B-scans forms the conventional SD-OCT intensity image. The amplitude decorrelation between these 2 B-scans forms the OCT-A image. Since the OCT-A image and SD-OCT intensity image are based on the same B-scans, there is pixel to pixel co-localization between the OCT-A image volume and SD-OCT intensity image, and no need for alignment. In addition, AnioVue system uses a Split-Spectrum Amplitude-Decorrelation Angiography (SSADA) method to capture the dynamic motion of the red blood cells and provide a high-resolution 3D visualization of perfused retinal microvasculature (Fig 1, Fig 2A-3 and B-3).[14, 21,24,25] The microvascular information is characterized at various user-defined retinal layers as a vessel density map. Then, vessel density (%) is calculated as the proportion of measured area occupied by flowing blood vessels (defined as pixels having decorrelation values acquired by the SSADA algorithm above the threshold level) (Fig 1, Fig 2A-3 and B-3).[21]

In the present study, circumpapillary vessel density (cpVD) was calculated in the RNFL and measured in a region defined as a 750-μm-wide elliptical annulus extending from the optic disc boundary based on the 360 degree global area and eight 45 degree sectors (Fig 1, Fig 2A-3 and B-3). [21]

Image quality review was performed on all scans according to a standard protocol established by the Imaging Data Evaluation and Analysis (IDEA) reading center at the Hamilton Glaucoma Center. Trained graders reviewed scans and those with poor image quality, as defined by the following criteria, were excluded: 1) a signal strength index < 48 (1= minimum, 100 = maximum), 2) poor clarity, 3) residual motion artifacts visible as irregular vessel pattern or disc boundary on the enface angiogram, 4) local weak signal, 5) RNFL segmentation errors. The delineation of the disc margin was reviewed for accuracy and adjusted manually, if required.[21]

Swept-Source Optical Coherence Tomography imaging

For detecting focal LC defects, optic disc was imaged with SS-OCT (DRI-OCT, Topcon, Tokyo, Japan). This device has an image-acquisition rate of 100,000 A-scans/second using a light source with a center wavelength of 1050 nm. Details on the device have been described elsewhere.[26–28]

A 3-dimensional (3D) raster scan consisting of 256 serial horizontal B- scans over 12 × 9 - mm cube centered on the posterior pole (wide-field protocol) was acquired,[28] and serial enface images were obtained from the 3D data set.

Poor quality images (quality score < 50, clipped or poorly focused scans) due to media opacity, irregular tear film, or inadequate patient cooperation were excluded.[28] Eyes with poor visibility of the LC, defined as < 70% visibility of the anterior laminar surface within the Bruch's membrane opening were also excluded from analysis.[9] Two independent observers masked to the clinical information of the study subjects (M.H.S and P.C.M) carefully reviewed the obtained horizontal and enface SS-OCT images for the presence of focal LC defects. Discrepancies between the two observers were resolved by consensus. If consensus could not be reached, the subject was excluded from the analysis. A focal LC defect was defined as a laminar hole or laminar disinsertions violating the normal U- or W-shaped contour of the anterior laminar surface.[6–11,29] To avoid false positives, focal LC defects were required to be ≥ 100 μm in diameter and > 30 μm in depth, and also to be present on at least 2 consecutive scans.[6, 7, 10, 11,29] Observers also confirmed that the candidate LC defects did not correspond with the hypo-reflectivity due to vascular shadowing by comparing the enface images with the disc photographs.

Location of the LC defect was described in terms of eight 45 degree sectors corresponding to the sectors on the SD-OCT Avanti and AngioVue instruments (Fig 2A-2, 3 and B-2, 3). An 8-sector face circle was placed around the ONH of the SS-OCT enface image after matching its location with that of the AngioVue cpVD circular diagram registering the images by matching the location of the vessels (Fig 2). Then, a sector in which the defect was located was assigned. If the subject had a LC defect located over two neighboring sectors, only one sector that involved the larger portion of a defect was assigned.

If both eyes of each POAG patient had focal LC defects or were free of focal LC defects, one eye from the patient was randomly selected for analysis. If a patient had one eye with and one eye without a focal LC defect, the eye with the focal LC defect was included. POAG subjects without a focal LC defect were matched to those with defects for VF mean deviation (MD) to minimize influence of the glaucoma severity on LC defect, cpRNFL thickness and vessel density. Specifically, patients with focal LC defects were matched to patients without LC defects into 3 groups based on the severity of their visual field damage, (27 early POAG (MD > −6 dB), 8 moderate POAG (−12 dB ≤ MD ≤− 6 dB), and 6 advanced POAG (MD < −12 dB)) by using frequency matching method.

Data analysis

Clinical characteristics, OCT-derived cpRNFL thicknesses, and OCT-A-derived vessel densities were compared between glaucomatous eyes with and without focal LC defects. Normality assumption was assessed by inspecting histograms and using Shapiro-Wilk tests. Independent samples student *t*-test was used for group comparison for normally distributed variables, Mann Whitney test for continuous non-normal variables, and Chi-squared test for categorical variables. To evaluate inter-observer agreement for the presence of focal LC defects, the kappa coeffient was calculated.[11, 30, 31] All statistical analyses were performed

with JMP version 11.2.0 (SAS Inc., Cary, NC) and MedCalc (MedCalc, Inc, Mariakerke, Belgium).The α level (type I error) was set at 0.05.

Results

Among 180 eyes of 138 POAG patients initially enrolled, 36 eyes from 21 patients were excluded due to poor quality OCT-A (34 eyes of 19 patients) or SD-OCT ONH (2 eyes of 2 patients) images. Among the remaining 144 eyes of the 117 patients, 6 eyes (4.2%) of 3 patients were excluded due to not having SS-OCT images, 13 eyes (9.0 %) of 11 patients due to poor quality SS-OCT images, and 1 eye (0.69 %) of 1 patient due to failure in reaching consensus between the two observers in determining the presence of a LC defect. There remained 55 eyes of 42 patients with LC defects and 69 eyes of 60 patients without a LC defect. After frequency matching VF MD between patients with and without LC defects, 41 eyes of 41 POAG patients were included in each group. There was an excellent inter-observer agreement in determining the presence of the LC defect in these 82 eyes (Kappa = 0.84, 95% CI 0.76–0.91, $P < 0.001$).[31]

Demographics and characteristics of ophthalmic measurements are summarized in Table 1. There were no significant differences between patients with and without LC defects in the baseline clinical and ocular characteristics including age, diabetes mellitus, systemic hypertension, systemic antihypertensive and diabetes medications, number and type of topical glaucoma medications, IOP, MOPP, presence of the disc hemorrhage, VF MD, and global and sectoral RNFL thicknesses ($P > 0.05$) (Table 1).

Among 41 eyes with focal LC defects, 33 (80 %) eyes had defects located in the inferotemporal (IT) sector, 19 (46 %) in the superotemporal (ST) sector, and 1 (2 %) in the inferonasal (IN) sector, and 1 (2%) in the in the superonasal (SN) sector. LC defects were detected in both ST and IT sectors in 12 (29 %) eyes and in both IN and IT sectors in 1 eye (2 %).

Table 2 presents the OCT-A-derived vessel densities according to the presence of LC defects. Eyes with focal LC defects had significantly lower cpVDs than those without a defect in global area (52.9 ± 5.6 vs. 56.8 ± 7.7 %, $P = 0.013$), and in the IT (49.5 ± 10.3 vs. 56.8 ± 12.2 %, $P = 0.004$), ST (54.3 ± 8.8 vs. 58.8 ± 9.6 %, $P = 0.030$), and IN (52.4 ± 9.0 vs. 57.6 ± 9.1 %, $P = 0.009$) sectors. The two groups did not differ significantly with respect to cpVDs of all other sectors ($P > 0.05$, Table 2).

Subgroup analysis of 33 eyes with LC defects in the IT sector showed significantly lower cpVDs than those without a defect in the IT and IN sectors, with sectoral differences highest in the IT (49.1 ± 10.3 vs. 56.8 ± 12.2 %, $P = 0.005$) followed by IN (53.0 ± 9.00 vs. 57.6 ± 9.1 %, $P = 0.035$) sectors (Fig 2 and 3A). The subset of 19 eyes with LC defects in the ST sector had lower cpVDs in the ST, IT, and IN sectors, and sector differences were highest in the ST (50.8 ± 9.4 vs. 58.8 ± 9.6 %, $P = 0.004$), followed by IT (49.1 ± 11.9 vs. 56.8 ± 12.2 %, $P = 0.026$), and IN (51.4 ± 10.4 vs. 57.9 ± 9.1 %, $P = 0.023$) sectors (Fig 3B). Mean global and sectoral cpRNFL thicknesses of the two subgroups with LC defects in ST and IT sectors did not differ from those without a defect ($P > 0.05$).

Discussion

In the present study, OCT-A based cpVDs measured in the RNFL were significantly lower in glaucomatous eyes with focal LC defects compared to eyes without LC defects, while glaucoma severity did not differ between the two groups. Lower cpVD was most pronounced in the superotemporal and inferotemporal sectors and, most importantly, showed a topographic relationship with the location of the LC defect. To our knowledge, this is the first study to evaluate the relationship between the retinal microvasculature and focal LC defects.

Lamina cribrosa is a porous structure through which RGC axons and retinal blood vessels pass,[2–4] and focal LC damage has been associated with axonal and vascular damage.[6–11] There is increasing evidence that various clinical signs of the axonal loss such as a RNFL defect, neuroretinal rim thinning/notching, and APON may be related to focal LC damage.[5, 7, 10, 11, 29] Until recently, the relationship between LC defects and retinal microvasculature has been difficult to evaluate since in-vivo imaging of the microvasculature at specific retinal layers was not possible. For example, it only could be inferred that a focal LC defect is related to the presence of a disc hemorrhage detected on the disc photographs.[7–9] With OCT-A, we now are able to demonstrate that peripapillary vessel density in eyes with similar severity of POAG was significantly lower when there is a focal LC defect than when there is not a LC focal defect. The current findings are consistent with previous studies suggesting that focal LC defects and impaired ocular hemodynamics may be etiologically related, and that mechanical and vascular mechanisms of glaucomatous optic nerve injury are inseparably intertwined.[12, 13]

The present study also confirms previous results that focal LC defects are located mostly in the IT area followed by the ST area of the ONH.[9, 11, 29] Similarly, significantly lower OCT-A-derived circumpapillary vessel density was notable in these areas. Furthermore, subgroup analysis on eyes with LC defects at ST and IT sectors showed that the location of the lowest vessel density corresponded topographically to the location of the LC defect. A subset of eyes with LC defects at the ST sector had lower vessel density in the contralateral IT and IN sectors as well as in the corresponding ST sector. This may be because 63.2 % (12/19) of those with LC defects in the ST area also had defects in the IT area. These findings suggest that detectable structural and microvascular damage to the optic disc are spatially correlated.[8] One possible explanation for the temporal relationship between the laminar and microvascular changes is that loss of structural support of the laminar beams due to the focal LC defect may directly or indirectly influence local retinal microvasculature.[3, 7, 33–35] Conversely, impaired vascular supply to the laminar beams may lead to the focal disruption of the laminar structures. These speculations cannot be confirmed in the present study because of its cross sectional design. Longitudinal studies are needed to elucidate the temporal relationship between the development of focal LC defects and reduced peripapillary vessel density.

The current OCT-A provides good quality images for the microvasculature located within the peripapillary RNFL, but not for those within the ONH deep structures due to projection artifacts in which the superficial blood vessels project to deeper tissue. Vessel density

specific to the neuroretinal rim tissue is also not provided with existing software. Moreover, our analysis is focused on the microvasculature within the circumpapillary RNFL, which is measured outside of the optic disc margin and, therefore, does not contain rim tissue. The measurement within the circumpapillary RNFL captures the radial peripapillary capillaries (RPCs), vessels suggested to play a role in the pathophysiology of POAG.[21, 36–39] Further studies with improved OCT-A assessment and objective criteria in determining the microvascular dropout in ONH structures are needed to further assess this hypothesis.

One may argue that adjustment for multiple testing should be applied for comparing each global area and sector-wise vessel density parameter between eyes with and without focal LC defect. In this study, eyes with focal LC defects had significantly lower cpVD than those without defects in the IT sector ($P = 0.004$) (Table 2) even after applying Bonferroni correction with cutoff P value of 0.005 which is known to be a conservative method of controlling multiple comparisons.[40] When a less stringent correction method introduced by Benjamini-Hochberg was applied,[41] global area (Adjusted $P = 0.043$), IN (Adjusted $P = 0.043$), and IT (Adjusted $P = 0.040$) sectors remained statistical significant. Therefore, it is less likely that differences of the cpVD values between eyes with and without focal LC defects were observed by chance.

Optic disc hemorrhage, a vascular parameter associated with the presence and progression of the glaucoma,[23] is known to be related to the presence of a focal LC defect.[7,8] However, in this study, the prevalence of the disc hemorrhage did not differ between eyes with and without defects. These results may be due to the relatively small number of disc hemorrhages (n = 11) detected in our study population. It is also possible that matching of the glaucomatous eyes with and without LC defects by glaucoma severity (VF MD) made the groups more similar with respect to RNFL thickness and/or presence of disc hemorrhages.[7, 14, 16] However, though not statistically significant, eyes with LC defects tended to have worse VF MDs (−6.60 ± 6.02 dB and −5.82 ± 6.08 dB, respectively, $P = 0.252$) and thinner RNFL (72.2 ± 10.2 μm and 73.7 ± 14.1 μm, respectively, for global cpRNFL thickness, $P = 0.576$) than those without a defect suggesting that influence of the axonal loss on the vessel density cannot be completely ruled out. Moreover, matching the glaucoma severity between eyes with and without focal LC defects resulted in an overlap in the distribution of the VF MDs, RNFL thickness, and vessel density values between the two groups. VF MDs and RNFL thicknesses were not significantly different between the two groups (by design). However, despite a large overlap in the cpVD values in eyes with and without LC defects, there was a significant difference between the 2 groups. The clinical utility of the difference is not clear. Longitudinal studies are needed to determine the temporal relationship between microvascular dropout and LC defects. Patient matching also led to a relatively small sample size, and thus may limit the generalizability of the current results to the general glaucoma population. Another limitation is that focal LC defects were based on subjective observation, and even with SS-OCT it is sometimes challenging to visualize the deep ONH structures.

However, this limitation was addressed at least in part by having two graders determine the presence of LC defects and by the excellent inter-observer agreement in determining the presence of the LC defect (Kappa = 0.84), and by the lower exclusion rate of the poor-

quality SS-OCT images (9.0 %) compared with previous studies ranging between 20.0 and 25.7 %.[8, 10, 11] The use of the enface SS-OCT images, which provided clearer visualization of the LC, may have contributed to the high inter-observer agreement and low exclusion rate of the current study.[9] Third, this study had relatively high number of poor quality OCT-A images (34/180 (18.9 %)). The current OCT-A is a newly introduced technique and does not have an eye tracking system. Approximately, 13.3 % (24/180) of scans in this study were excluded due to excessive movement. Further application of the eye tracking system may help obtain better quality OCT-A images. Fourth, the current OCT-A technique generates binary image of the vessels based on the amplitude decorrelation between rapidly repeated B-scans. Therefore, vessels without flow may not be visualized due to lack of motion contrast. Finally, usage of two different devices and relatively large 8 sectors may not facilitate accurate registration between the location of the focal LC defect and vessel density reduction. The current OCT-A software only provides circumpapillary RNFL vessel density globally and in 8 fixed 45º sectors. Moreover, the current SD-OCT (Avanti) in which OCT-A (AngioVue) software is incorporated does not have an enhanced depth imaging technique that allows detailed analysis on the laminar structure, therefore we utilized SS-OCT for the lamina analysis. However, the OCT-A image is directly derived from SD-OCT B-scans. Moreover, because SS-OCT and SD-OCT images were aligned by matching the large vessels, it is unlikely that there is a significant error in evaluating the topographical relationship between vessel density and focal LC defects. Further development of the OCT-A software that allows for location specific vessel density measures and enhanced depth imaging are needed to more precisely map the location of microvasculature dropout to lamina defects.

In conclusion, circumpapilllary vessel density was significantly lower in glaucomatous eyes with focal LC defects than those without focal LC defects, especially in superotemporal and inferotemporal sectors. Moreover, lower vessel density was spatially correlated with the location of the LC defect. Longitudinal studies are needed to determine the temporal relationship between the structural alteration of the LC and the retinal microvasculature.

Acknowledgments

This work was supported in part by National Institutes of Health/Nation Eye Institute grants P30EY022589, EY11008, EY019869, EY021818, Inje University research grant, and an unrestricted grant from Research to Prevent Blindness (New York, NY).

References

1. Weinreb RN, Aung T, Medeiros FA. The pathophysiology and treatment of glaucoma: a review. JAMA. 2014; 311(18):1901–11. [PubMed: 24825645]
2. Fechtner RD, Weinreb RN. Mechanisms of optic nerve damage in primary open angle glaucoma. Surv Ophthalmol. 1994; 39(1):23–42. [PubMed: 7974188]
3. Anderson DR. Ultrastructure of human and monkey lamina cribrosa and optic nerve head. Arch Ophthalmol. 1969; 82(6):800–14. [PubMed: 4982225]
4. Wilczek M. THE LAMINA CRIBROSA AND ITS NATURE. Br J Ophthalmol. 1947; 31(9):551–65. [PubMed: 18170379]
5. Quigley HA, Addicks EM. Regional differences in the structure of the lamina cribrosa and their relation to glaucomatous optic nerve damage. Arch Ophthalmol. 1981; 99(1):137–43. [PubMed: 7458737]

6. Faridi OS, Park SC, Kabadi R, et al. Effect of Focal Lamina Cribrosa Defect on Glaucomatous Visual Field Progression. Ophthalmology. 2014; 121(8):1524–30. [PubMed: 24697910]
7. Park SC, Hsu AT, Su D, et al. Factors Associated With Focal Lamina Cribrosa Defects in Glaucoma. Investigative Opthalmology & Visual Science. 2013; 54(13):8401.
8. Lee EJ, Kim TW, Kim M, et al. Recent structural alteration of the peripheral lamina cribrosa near the location of disc hemorrhage in glaucoma. Invest Ophthalmol Vis Sci. 2014; 55(4):2805–15. [PubMed: 24677111]
9. Kim YK, Park KH. Lamina cribrosa defects in eyes with glaucomatous disc haemorrhage. Acta Ophthalmologica. 2015 n/a-n/a.
10. You JY, Park SC, Su D, et al. Focal Lamina Cribrosa Defects Associated With Glaucomatous Rim Thinning and Acquired Pits. JAMA Ophthalmology. 2013; 131(3):314. [PubMed: 23370812]
11. Tatham AJ, Miki A, Weinreb RN, et al. Defects of the Lamina Cribrosa in Eyes with Localized Retinal Nerve Fiber Layer Loss. Ophthalmology. 2014; 121(1):110–8. [PubMed: 24144452]
12. Burgoyne CF, Crawford Downs J, Bellezza AJ, et al. The optic nerve head as a biomechanical structure: a new paradigm for understanding the role of IOP-related stress and strain in the pathophysiology of glaucomatous optic nerve head damage. Progress in Retinal and Eye Research. 2005; 24(1):39–73. [PubMed: 15555526]
13. Downs, C., Roberts, MD., Burgoyne, CF. Mechanical strain and restructuring of the optic nerve head. In: Shaarawy, TM.Sherwood, MB.Hitchings, RA., Crowston, JG., editors. Glaucoma Medical Diagnosis and Therapy. Vol. 1. Philadelphia, PA: Saunders Elsevier; 2009.
14. Jia Y, Wei E, Wang X, et al. Optical Coherence Tomography Angiography of Optic Disc Perfusion in Glaucoma. Ophthalmology. 2014; 121(7):1322–32. [PubMed: 24629312]
15. Liu L, Jia Y, Takusagawa HL, et al. Optical Coherence Tomography Angiography of the Peripapillary Retina in Glaucoma. JAMA Ophthalmology. 2015; 133(9):1045. [PubMed: 26203793]
16. Wang X, Jiang C, Ko T, et al. Correlation between optic disc perfusion and glaucomatous severity in patients with open-angle glaucoma: an optical coherence tomography angiography study. Graefe's Archive for Clinical and Experimental Ophthalmology. 2015; 253(9):1557–64.
17. Aizawa N, Yokoyama Y, Chiba N, et al. Reproducibility of retinal circulation measurements obtained using laser speckle flowgraphy-NAVI in patients with glaucoma. Clin Ophthalmol. 2011; 5:1171–6. [PubMed: 21887100]
18. Nicolela MT, Hnik P, Schulzer M, Drance SM. Reproducibility of retinal and optic nerve head blood flow measurements with scanning laser Doppler flowmetry. J Glaucoma. 1997; 6(3):157–64. [PubMed: 9211138]
19. Iester M, Altieri M, Michelson G, et al. Intraobserver reproducibility of a two-dimensional mapping of the optic nerve head perfusion. J Glaucoma. 2002; 11(6):488–92. [PubMed: 12483092]
20. Hitchings RA, Spaeth GL. Fluorescein angiography in chronic simple and low-tension glaucoma. Br J Ophthalmol. 1977; 61(2):126–32. [PubMed: 843509]
21. Yarmohammadi A, Zangwill LM, Diniz-Filho A, et al. Optical coherence tomography angiography vessel density in healthy, glaucoma suspects, and glaucoma. Invest Ophthalmol Vis Sci. 2016 In press.
22. Sample PA, Girkin CA, Zangwill LM, et al. The African Descent and Glaucoma Evaluation Study (ADAGES): design and baseline data. Arch Ophthalmol. 2009; 127(9):1136–45. [PubMed: 19752422]
23. Suh MH, Park KH. Pathogenesis and clinical implications of optic disk hemorrhage in glaucoma. Survey of Ophthalmology. 2014; 59(1):19–29. [PubMed: 24156914]
24. Jia Y, Tan O, Tokayer J, et al. Split-spectrum amplitude-decorrelation angiography with optical coherence tomography. Opt Express. 2012; 20(4):4710–25. [PubMed: 22418228]
25. Jia Y, Morrison JC, Tokayer J, et al. Quantitative OCT angiography of optic nerve head blood flow. Biomed Opt Express. 2012; 3(12):3127–37. [PubMed: 23243564]
26. Mansouri K, Medeiros FA, Marchase N, et al. Assessment of choroidal thickness and volume during the water drinking test by swept-source optical coherence tomography. Ophthalmology. 2013; 120(12):2508–16. [PubMed: 24021895]

27. Yasuno Y, Hong Y, Makita S, et al. In vivo high-contrast imaging of deep posterior eye by 1-microm swept source optical coherence tomography and scattering optical coherence angiography. Opt Express. 2007; 15(10):6121–39. [PubMed: 19546917]
28. Zhang C, Tatham AJ, Medeiros FA, et al. Assessment of Choroidal Thickness in Healthy and Glaucomatous Eyes Using Swept Source Optical Coherence Tomography. PLoS ONE. 2014; 9(10):e109683. [PubMed: 25295876]
29. Kiumehr S, Park SC, Syril D, et al. In vivo evaluation of focal lamina cribrosa defects in glaucoma. Arch Ophthalmol. 2012; 130(5):552–9. [PubMed: 22232364]
30. Cohen J. Weighted kappa: nominal scale agreement with provision for scaled disagreement or partial credit. Psychol Bull. 1968; 70(4):213–20. [PubMed: 19673146]
31. Landis JR, Koch GG. An application of hierarchical kappa-type statistics in the assessment of majority agreement among multiple observers. Biometrics. 1977; 33(2):363–74. [PubMed: 884196]
32. Burgoyne CF. A biomechanical paradigm for axonal insult within the optic nerve head in aging and glaucoma. Experimental Eye Research. 2011; 93(2):120–32. [PubMed: 20849846]
33. Mackenzie PJ, Cioffi GA. Vascular anatomy of the optic nerve head. Can J Ophthalmol. 2008; 43(3):308–12. [PubMed: 18443611]
34. Guidoboni G, Harris A, Carichino L, et al. Effect of intraocular pressure on the hemodynamics of the central retinal artery: a mathematical model. Math Biosci Eng. 2014; 11(3):523–46. [PubMed: 24506550]
35. Guidoboni G, Harris A, Cassani S, et al. Intraocular pressure, blood pressure, and retinal blood flow autoregulation: a mathematical model to clarify their relationship and clinical relevance. Invest Ophthalmol Vis Sci. 2014; 55(7):4105–18. [PubMed: 24876284]
36. Henkind P. Radial peripapillary capillaries of the retina. I. Anatomy: human and comparative. Br J Ophthalmol. 1967; 51(2):115–23. [PubMed: 4959937]
37. Henkind P, Bellhorn RW, Poll D. Radial peripapillary capillaries. 3. Their development in the cat. Br J Ophthalmol. 1973; 57(8):595–9. [PubMed: 4743924]
38. Kornzweig AL, Eliasoph I, Feldstein M. Selective atrophy of the radial peripapillary capillaries in chronic glaucoma. Arch Ophthalmol. 1968; 80(6):696–702. [PubMed: 4177355]
39. Yu PK, Cringle SJ, Yu DY. Correlation between the radial peripapillary capillaries and the retinal nerve fibre layer in the normal human retina. Exp Eye Res. 2014; 129:83–92. [PubMed: 25447563]
40. Perneger TV. What's wrong with Bonferroni adjustments. BMJ. 1998; 316(7139):1236–8. [PubMed: 9553006]
41. Benjamini YH. Yosef Cntrolling the false discovery rate: a practical and powerful approach in multiple testing. Journal of the Royal Society, Series B. 1995; 57(1):289–300.

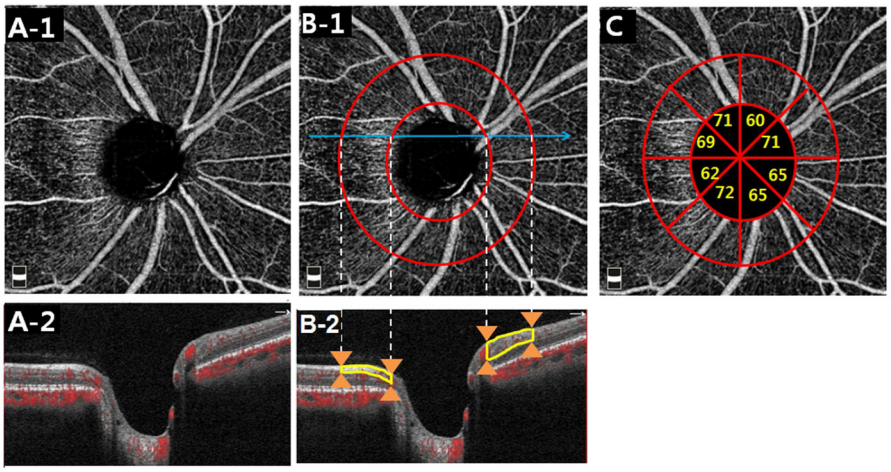

Figure 1.

Analysis of the circumpapillary retinal nerve fiber layer vessel density (cpVD) based on optic nerve head optical coherence tomography angiography images. **A,** Enface **(A-1)** and horizontal **(A-2)** images of the radial peripapillary capillaries within the retinal nerve fiber (RNFL) layer. **B-1**, Same enface image as **A-1**, but annotated to indicate a 750 μm-wide elliptical annulus (red circles) extending from the optic disc boundary which forms the region of analysis for cpVD and the location of the B-scan shown in **B-2** (sky blue lines). **B-2,** B-scan view of the vessel density analysis region located within the elliptical annulus (orange arrows) and within the depth range of the RNFL layer (yellow outlines). **C**, Same enface image as **A** and **B-1**, but annotated to indicate for eight 45 degree sectors for cpVD.

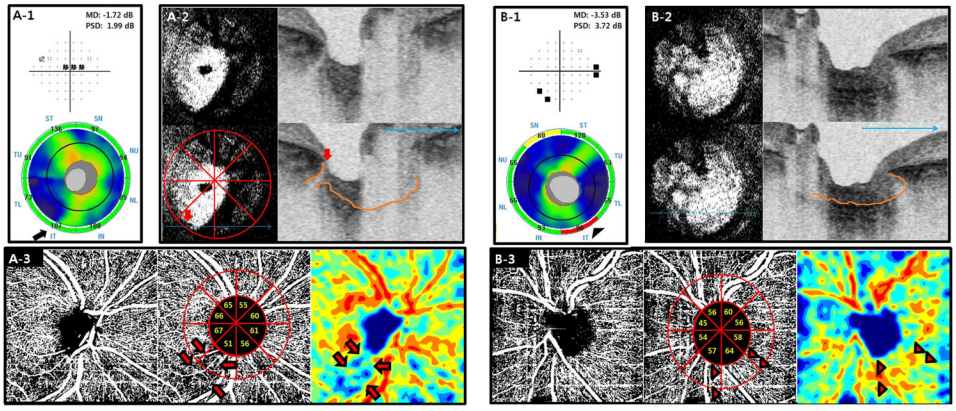

Figure 2.

Optical coherence tomography angiography (OCT-A)-derived vessel density map in primary open angle glaucoma subjects with (**A**) and without (**B**) a focal lamina cribrosa (LC) defect. **A-1 and B-1**, Visual field (**top**) and circumpapillary retinal nerve fiber layer (RNFL) thickness on the spectral-domain OCT (**bottom**) of the right eye with a focal LC defect (**A-1**) and left eye without a defect (**B-1**). Note that the eye with a LC defect did not show RNFL thinning (all RNFL sectors were within normal limits) on the circular diagram (black arrow) (**A-1 bottom**), while an eye without a defect showed an RNFL defect (outside normal limit) in the inferotemporal (IT) sector (black arrowhead) (**B-1 bottom**). **A-2 and B-2**, Enface (**left**) and horizontal (**right**) B-scan images of the swept source (SS)-OCT from an eye with (**A-2**) and without (**B-2**) a LC defect. Bottom images are the same as top images without labels, and contain a 8-sector face circle, orange lines delineating anterior LC surface, and large sky blue arrows indicating the horizontal scan direction. A focal LC defect was located in the IT sector (red arrows) on SS-OCT (**A-2**). **A-3 and B-3**, Circumpapillary RNFL vessel density map of an eye with (**A-3**) and without (**B-3**) a LC defect. Center images are the same as left images but are annotated to include the 8-sector circle with vessel density values for each sector. Right images show color-coded maps. The eye with a LC defect showed notable vessel density reduction (black outlined red arrows) in the corresponding IT sector (**A-3**), while an eye without a defect showed no evidence of focal vessel density reduction in the IT sector (black outlined red arrowheads) (**B-3**). TU = upper temporal sector; ST = superotemporal sector; SN = superonasal sector; NU = upper nasal sector; NL = lower nasal sector; IN = inferonasal sector; IT = inferotemporal sector; TL = lower temporal sector.

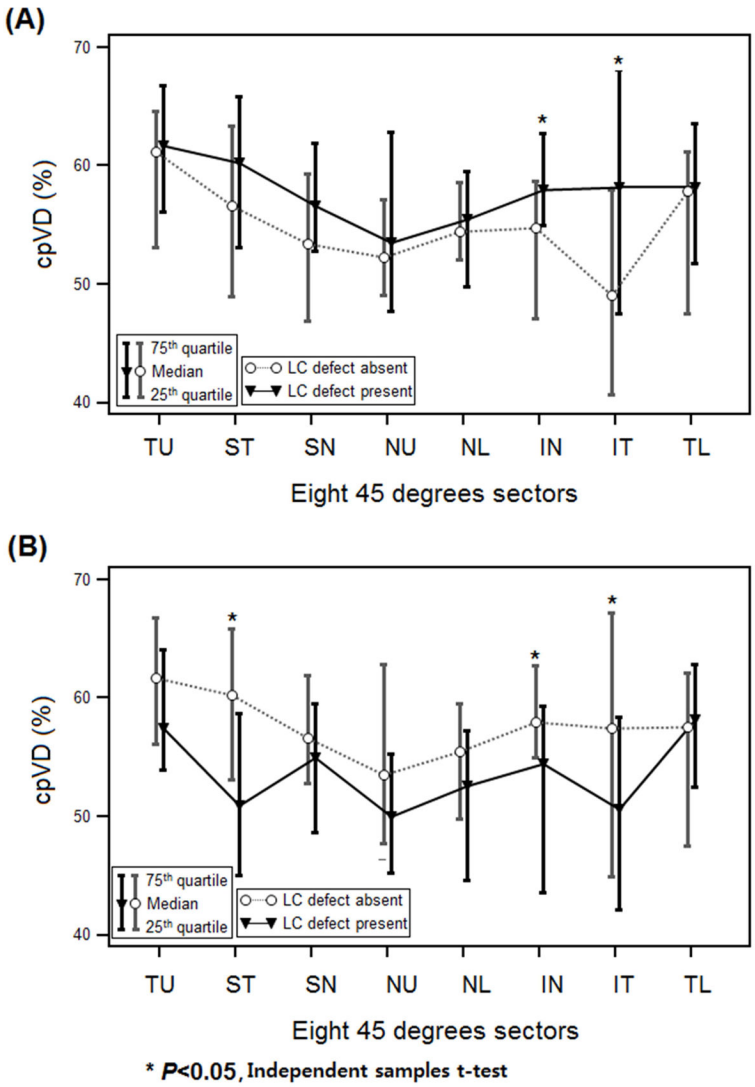

Figure 3.

Comparison of OCT-A circumpapillary vessel density (cpVD) profiles between glaucomatous eyes with and without a focal lamina cribrosa (LC) defect. **A,** A subset of 33 eyes with a LC defect located in the IT sector had significantly lower cpVDs in the IT and IN sectors compared with those without a defect. Sector differences were highest in the IT sector. **B,** A subset of 19 eyes with a LC defect in the ST sector had significantly lower cpVDs in the ST, IN and IT sectors compared with those without a defect. Sector differences were highest in the ST sector. IT = inferotemporal sector; NL = lower nasal sector; NU = upper nasal sector; SN = superonasal sector; ST = superotemporal sector; TL = lower temporal sector; TU = upper temporal sector.

Table 1

Subject demographics and baseline clinical characteristics.

Variables	Eyes with Focal LC Defect (41 eyes, 41 patients)	Eyes without Focal LC Defect (41 eyes, 41 patients)	*P*-value
Age (years)	73.4±14.0 (36 to 94)	72.0±9.5 (51 to 89)	0.235 *
Gender (male/female)	20/21	24/17	0.507 †
SE (D)	−0.95±2.2 (−8.4 to 2.3)	−0.94±1.7 (−5.1 to 2.9)	0.568 *
CCT (μm)	529.1±42.3 (460.3 to 606.0)	532.3±40.7 (425.3 to 619.0)	0.739 ‡
Ethnicity (ASD/ED/AFD)	9/24/8	3/29/9	0.171 †
Self-reported diabetes, n (%)	6 (14.6 %)	4 (9.8 %)	0.736 †
Self-reported hypertension, n (%)	22 (53.7 %)	19 (46.3 %)	0.659 †
Antihypertensive medication, n (%)	17 (41.5 %)	16 (39.0 %)	1.000 †
Diabetes medication, n (%)	5 (12.2 %)	3 (7.3 %)	0.710 †
Number of topical glaucoma medications, n (%)			
0	1 (2.4 %)	4 (9.8 %)	0.246 †
1	16 (39.0 %)	11 (26.8 %)	
>1	24 (58.5 %)	26 (63.4 %)	
Topical medications, n			
Prostaglandin analogues	31	30	0.990 †
Beta-antagonists	16	17	
Carbonic anhydrase inhibitors	6	7	
Alpha-1-antagonists	20	20	
IOP (mmHg)	13.5±5.7 (4 to 30)	13.1±4.4 (4 to 26)	0.787 ‡
SBP (mmHg)	127.1±14.2 (92 to 162)	121.9±12.8 (98 to 151)	0.083 ‡
DBP (mmHg)	77.5±11.3 (51 to 108)	75.9±9.2 (51 to 100)	0.474 ‡
MOPP (mmHg)	54.7±8.6 (35.1 to 75.8)	52.5±6.2 (39.3 to 66.7)	0.197 ‡
Pulse rate (bpm)	67.9±12.4 (46 to 108)	66.0±11.4 (41 to 85)	0.767 *
Disc hemorrhage, n (%)	4 (9.8 %)	7 (17.1 %)	0.517 †
VF MD (dB)	−6.60±6.02 (−25.87 to −0.41)	−5.82±6.08 (−26.24 to −0.30)	0.252 *
VF PSD (dB)	6.60±3.96 (1.71 to 14.57)	5.63±3.69 (1.82 to 14.37)	0.286 *
Disc area (mm^2)	2.2±0.4 (1.4 to 3.2)	2.0±0.53 (0.93 to 3.0)	0.156 ‡
RNFL thickness			
Global area (μm)	72.2±10.2 (51.9 to 98.9)	73.7±14.1 (41.5 to 110.7)	0.576 ‡
Upper temporal (μm)	60.4±14.7 (31.6 to 93.8)	60.0±15.4 (31.7 to 86.7)	0.895 ‡
Upper nasal (μm)	64.6±12.8 (43.2 to 98.7)	62.9±13.1 (32.0 to 105.5)	0.558 ‡
Lower nasal (μm)	61.3±11.2 (36.9 to 88.1)	59.8±11.1 (35.8 to 81.6)	0.554 ‡
Lower temporal (μm)	53.6±9.7 (35.7 to 84.8)	55.0±14.4 (28.1 to 103.6)	0.608 ‡

Variables	Eyes with Focal LC Defect (41 eyes, 41 patients)	Eyes without Focal LC Defect (41 eyes, 41 patients)	*P*-value
Superotemporal (μm)	95.2±21.0 (56.0 to 136.3)	97.0±23.3 (50.2 to 144.1)	0.714‡
Superonasal (μm)	81.9±14.7 (48.2 to 113.9)	81.9±20.8 (52.3 to 138.0)	0.901‡
Inferonasal (μm)	80.3±20.4 (48.8 to 139.3)	84.7±23.1 (40.7 to 135.7)	0.366 ‡
Inferotemporal (μm)	80.6±21.4 (50.9 to 127.9)	88.1±25.7 (46.6 to 142.6)	0.154 *

Continuous variables are shown in mean ± standard deviation (range).

*The comparison was performed by using Mann-Whitney test.

†The comparison was performed by using Chi-squared test.

‡The comparison was performed by using independent samples t-test.

SE = spherical equivalent; CCT = central corneal thickness; ASD = Asian descent; ED = European descent; AFD = African descent; IOP = intraocular pressure; SBP = systolic blood pressure; DBP = diastolic blood pressure; MOPP = mean ocular perfusion pressure; VF MD = visual field mean deviation; VF PSD = visual field pattern standard deviation; RNFL = retinal nerve fiber layer.

Table 2

Comparison of the optical coherence tomography angiography (OCT-A)-derived circumpapillary vessel density values between the primary open angle glaucoma subjects with and without a focal lamina cribrosa (LC) defect in global area and in eight 45 degrees sectors.

	Eyes with Focal LC Defect (41 eyes, 41 patients)		Eyes without Focal LC Defect (41 eyes, 41 patients)	*P*-value
	N*	OCT-A parameters (%)	OCT-A parameters (%)	
Global area	-	52.9±5.6 (42.4 to 63.1)	56.8±7.7 (35.4 to 71.5)	**0.013**†
Upper temporal	0	57.1±9.9 (32.9 to 72.6)	60.0±9.9 (38.0 to 73.4)	0.107‡
Upper nasal	0	50.9±6.9 (33.6 to 62.5)	54.1±9.2 (31.9 to 71.4)	0.077†
Lower nasal	0	52.7±6.9 (36.4 to 63.3)	52.7±6.9 (32.3 to 66.9)	0.383†
Lower temporal	0	54.2±9.3 (34.8 to 70.9)	57.1±9.4 (29.7 to 74.8)	0.155†
Superotemporal	19	54.3±8.8 (33.7 to 69.7)	58.8±9.6 (33.8 to 73.1)	**0.030**†
Superonasal	1	53.5±6.7 (40.3 to 65.8)	55.9±7.9 (30.2 to 70.4)	0.133†
Inferonasal	1	52.4±9.0 (33.2 to 66.7)	57.6±9.1 (32.3 to 74.1)	**0.009**†
Inferotemporal	33	49.5±10.3 (28.0 to 66.8)	56.8±12.2 (31.8 to 76.0)	**0.004**†

Continuous variables are shown in mean ± standard deviation (range).

*N = number of eyes with focal LC defects in each of eight 45 degree sectors.

†The comparison of the OCT-A parameters was performed between eyes with and without a focal LC defect by using independent samples t-test.

‡The comparison of the OCT-A parameters was performed between eyes with and without a focal LC defect by using Mann-Whitney test.

Significant values are in bold type.